



Original Article

Cardiothoracic Morphology Measures in Heart Failure Patients to Inform Device Designs

MONA SAFFARZADEH,^{1,2} JAMES P. GAIEWSKY,^{1,2} JOSHUA TAN,² RYAN LAHM,³ BHARATHI UPADHYA,²
GEOFFREY T. JAO,² and ASHLEY A. WEAVER ^{1,2}

¹Virginia Tech-Wake Forest University School of Biomedical Engineering and Sciences, 575 N. Patterson Ave., Suite 120, Winston-Salem, NC 27101, USA; ²Wake Forest School of Medicine, Medical Center Blvd, Winston-Salem, NC 27157, USA; and ³Medtronic, Minneapolis, MN 55432-5604, USA

(Received 27 February 2019; accepted 5 October 2019; published online 21 October 2019)

Associate Editor Gautam Kumar oversaw the review of this article.

Abstract

Purpose—Approximately 5.7 million people in the US are affected by congestive heart failure. This study aimed to quantitatively evaluate cardiothoracic morphology and variability within a cohort of heart failure patients for the purpose of optimally engineering cardiac devices for a variety of heart failure patients.

Methods—Co-registered cardiac-gated and non-gated chest computed tomography (CT) scans were analyzed from 20 heart failure patients (12 males; 8 females) who were primarily older adults (79.5 ± 8.8 years). Twelve cardiothoracic measurements were collected and compared to study sex and left ventricular (LV) ejection fraction (EF) type differences in cardiothoracic morphology.

Results—Four measures were significantly greater in males compared to females: LV long-axis length, LV end diastolic diameter (LVEDD) at 50% length of the LV long-axis, the minimal distance between the sternum and heart, and the angle between the LV long-axis and coronal plane. Four measures were significantly greater in patients with reduced EF compared to preserved LV: LV long-axis length, LVEDD at 50% length of the LV long-axis, left ventricular volume normalized by body surface area, and the angle between the mitral valve plane and LV long-axis.

Conclusions—These cardiothoracic morphology measurements are important to consider in the design of cardiac devices for heart failure management (e.g. cardiac pacemakers,

ventricular assist devices, and implantable defibrillators), since morphology differs by sex and ejection fraction.

Keywords—Cardiac device, Computational models, Computed tomography, Ejection fraction, Electrocardiogram gated computed tomography, Heart failure.

INTRODUCTION

Approximately 5.7 million people in the US are affected by congestive heart failure (CHF) which remains the only cardiovascular disease with an increasing healthcare cost burden.⁵ CHF is a well-recognized condition in which left ventricular (LV) dysfunction produces symptoms including fatigue and exercise intolerance.⁶ The LV ejection fraction (EF) is the standard clinical measure of systolic function. HF occurs across the entire range of LV EF, not just reduced EF.¹⁸ Nearly half or more of HF patients have a preserved EF $\geq 50\%$.¹⁶ A preserved EF indicates that the end-diastolic volume is appropriate for the stroke volume, and a reduced EF indicates that the end-diastolic volume is increased relative to stroke volume.¹⁴ In addition, there are many differences in cardiac structure and function between these two groups.²⁵

Most structural studies of the heart use magnetic resonance imaging or echocardiography for LV mass and volume measurements.^{3,15,20,25} Cardiovascular magnetic resonance is costly, time-consuming, and unsuitable for patients with metallic devices or claustrophobia. Transthoracic echocardiography is an

Address correspondence to Ashley A. Weaver, Virginia Tech-Wake Forest University School of Biomedical Engineering and Sciences, 575 N. Patterson Ave., Suite 120, Winston-Salem, NC 27101, USA. Electronic mail: msaffarz@wakehealth.edu, jgaewsky@wakehealth.edu, jtan@wakehealth.edu, ryan.lahm@medtronic.com, bupadhya@wakehealth.edu, gtjao@wakehealth.edu, asweaver@wakehealth.edu

inexpensive, routine method for ventricular function assessment, but is limited by poor acoustic windows in patients with obesity, prior cardiothoracic surgery, chronic obstructive pulmonary disease, or narrow rib intercostal spaces.^{2,7,8}

Computed tomography (CT) is a recommended imaging modality for evaluation of ventricular function and morphology for HF patients.²¹ CT is routinely collected for surgical pre-planning, and can be rapidly acquired with good spatial and temporal resolution and a large field of view.^{1,4,19} Electrocardiogram (ECG) gated CT minimizes artifacts from cardiac motion and offers improved temporal resolution to characterize morphology of the heart valves and great vessels.¹⁰ By co-registering cardiac-gated heart CT images with non-gated chest CT images, precise morphological characterization of the heart and surrounding anatomy can be achieved by taking advantage of reduced heart motion artifacts in the gated CT and the larger field of view in the non-gated CT. Although magnetic resonance imaging is the gold standard and echocardiography is the most commonly used technique for HF image analysis, cardiac CT brings its own advantages in specific HF population studies since it is feasible for a broader range of patients. For example, shorter acquisition time of cardiac CT images leading to shorter breath-hold time makes it more feasible for HF patients with respiratory problems. Also, the increasing use of implantable cardioverter defibrillator/cardiac resynchronization therapy devices in HF patients, limits the possibilities of performing cardiac magnetic resonance imaging; thus CT emerges as a valid alternative to assess LV volumes and function.

The heart size, location, and orientation in the thoracic cavity likely varies among HF patients. Quantitative data on cardiothoracic morphology variations can directly inform the design of cardiac devices such as pacemakers, ventricular assist devices, and implantable defibrillators, as engineers must develop devices with widespread applicability to the HF population. Thus, the objective of this study was to generate 3D models of cardiothoracic organs from co-registered ECG-gated and non-gated chest CT scans of 20 HF patients. This data aimed to (1) improve the understanding of cardiothoracic morphology of HF patients, and (2) quantify variability of cardiothoracic morphology by sex and EF classification for the purpose of informing cardiac device design for HF patients.

MATERIALS AND METHODS

Model Development

Paired cardiac-gated CT and non-gated chest CT scans from 12 males and 8 females with HF were re-

trieved from the clinical radiology database at Wake Forest Baptist Medical Center (Table 1). The study complied with Institutional Review Board policies approved by Wake Forest University. The 20 patients were primarily older adults (79.5 ± 8.8 years) with a mean body mass index (BMI) of 26.9 ± 6.1 kg/m² and a mean body surface area (BSA) of 1.8 ± 0.2 m², which is commonly used to eliminate confounding effects of body size on cardiac dimensions⁹ (Eq. 1).

$$BSA = \frac{\sqrt{\text{Weight (kg)} \times \text{Height (cm)}}}{3600} \quad (1)$$

Patients selected had a contrast-enhanced cardiac-gated CT scan of the heart and a contrast-enhanced full chest CT scan performed during the same hospital admission. HF classified in these patients according to the New York Heart Association (NYHA) Functional Classification²⁴ included class II ($n = 1$), class III ($n = 16$), class IV ($n = 2$), and unspecified ($n = 1$). EF measured using transthoracic echocardiogram was stratified based on the maximum EF measured in each patient: preserved EF (EF $\geq 50\%$) ($n = 13$) vs. reduced EF (EF $< 50\%$) ($n = 7$).

Cardiac-gated CT (0.625 mm slice thickness; 0.59 mm pixel size) and non-gated chest CT (0.625 mm slice thickness; 0.95 mm pixel size) scans were collected on a 64-slice General Electric CT scanner (*GE Healthcare, Chicago, IL*). To minimize motion artifacts in the cardiothoracic measurements collected, cardiac-gated scans were collected at end diastole at 75% of the R-R interval during the cardiac cycle using retrospective gating.²²

The following heart structures were semi-automatically segmented from the cardiac-gated CT scan using the CT Heart tool within Mimics software (*v.19.01, Materialise, Ann Arbor, MI*): right and left atria, right and left ventricles, aorta, pulmonary arteries, pulmonary veins, coronary arteries, coronary sinus, superior vena cava, and myocardium. The following bone and soft tissue structures were semi-automatically segmented from the non-gated chest CT scans using Mimics: clavicles, sternum, ribs, costal cartilage, lungs, liver, diaphragm, esophagus, trachea, inferior vena cava, skeletal muscle, skin, and subcutaneous fat. Bones were segmented by thresholding for Hounsfield units (HU) ranging from 226 to 3071 HU, followed by manual refinement. Soft tissue structures in the non-gated CT were segmented using a combination of thresholding and manual contouring. 3D stereolithography models of each anatomical structure were created using optimal settings in Mimics and then smoothed in Geomagic Studio (*v.2014, Geomagic Inc., Morrisville, NC*).

TABLE 1. Demographic summary for 20 HF patients.

ID	Sex	Age (years)	Weight (kg)	Height (cm)	BMI (kg/m ²)	BSA (m ² , Eq. 1)	NYHA class	Ejection fraction	BP (mmHg)
1	F	88	70.8	149.9	31.5	1.7	III	70% (preserved)	144/50
2	M	89	76.7	169.4	27.3	1.9	III	65% (preserved)	134/54
3	F	93	54.0	148.7	24.9	1.5	III	64% (preserved)	165/72
4	F	87	100.2	151.3	43.9	2.1	III	60% (preserved)	182/77
5	M	80	71.4	166.7	26.2	1.8	III	60% (preserved)	136/63
6	F	78	57.7	156.7	24.1	1.6	III	45% (reduced)	109/50
7	F	86	46.3	159.3	18.7	1.4	III	70% (preserved)	138/47
8	M	83	68.5	166.9	25.2	1.8	N/R	50% (preserved)	142/70
9	F	87	58.0	154.2	25.0	1.6	IV	59% (preserved)	138/42
10	M	80	85.3	174.5	28.7	2.0	III	45% (reduced)	150/60
11	M	65	79.4	179.6	25.1	2.0	III	30% (reduced)	93/42
12	M	58	44.9	156.7	18.6	1.4	III	43% (reduced)	115/65
13	M	81	87.1	174.5	29.1	2.1	III	65% (preserved)	148/79
14	M	79	75.8	179.6	24.0	1.9	III	55% (preserved)	122/61
15	M	82	76.2	169.4	27.2	1.9	II	55% (preserved)	130/69
16	F	71	51.7	146.2	27.4	1.4	III	19% (reduced)	128/58
17	M	80	69.4	177.1	22.5	1.8	III	45% (reduced)	112/64
18	M	83	72.1	179.6	22.8	1.9	III-IV	30% (reduced)	104/77
19	F	68	99.8	159.3	40.4	2.1	III	65% (preserved)	101/46
20	M	72	74.8	174.5	25.1	1.9	III	55% (preserved)	153/67
Mean ± SD		79.5 ± 8.8	71.0 ± 15.6	164.7 ± 11.4	26.9 ± 6.1	1.8 ± 0.2		50.8 ± 13.5	

BMI body mass index, BSA body surface area, NYHA New York Heart Association, BP blood pressure, N/R not reported.

The cardiac-gated CT had a smaller field of view that did not capture the entire torso. Thus, the heart model from the cardiac-gated CT was rigidly co-registered to the non-gated full chest CT using a similar approach to Hayes *et al.*¹¹ This produced 3D models of all torso structures in the full chest CT coordinate system, complete with a heart segmentation derived from cardiac-gated CT (Fig. 1).

Cardiothoracic Measurements

For each patient, six cardiac and six cardiothoracic measurements were collected from 2D CT images using Aquarius iNtuition (v.4.4.11, TeraRecon, Foster City, CA, USA) and from the 3D models (Fig. 1) using Geomagic Studio (v.2014, Geomagic Inc., Morrisville, NC).

Cardiac Measures

The following cardiac measures relating to cardiac function were collected: (1) LV long-axis length, (2) left ventricular end diastolic diameter (LVEDD) at 50% of LV long-axis length, (3) LV short-axis length, (4) LV sphericity (defined as LV long-axis length divided by LV short-axis length), (5) four chamber volumes, and (6) LV myocardial wall volume divided by BSA (Figs. 2 and 3).

LV long-axis length was measured on the four-chamber view, from the LV apex to the central mitral

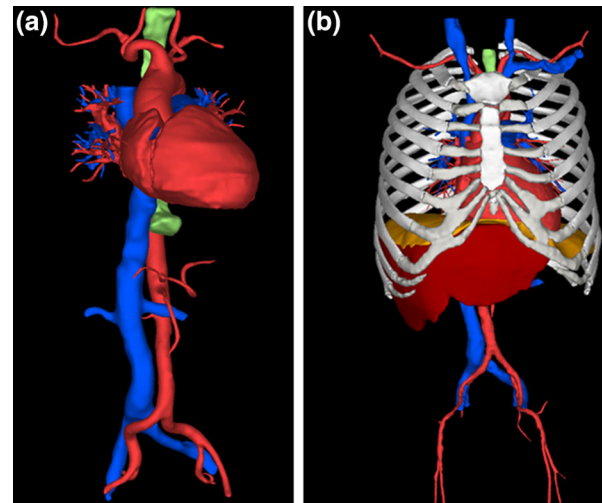


FIGURE 1. 3D models of (a) the heart and great vessels, (b) the cardiothoracic structures including bones and soft tissues.

valve (Fig. 2a). LVEDD at 50% of LV long-axis length was measured on the four-chamber view by crossing a line perpendicular to the LV long-axis at 50% of its length¹⁷ (Fig. 2b). LV short-axis length was measured on the apical two-chamber view (Fig. 2c).¹³ LV sphericity was calculated by dividing the LV long-axis length by the LV short-axis length. Four chamber volumes (LV volume, left atrial volume, right ventricular volume, and right atrial volume) were measured from 3D models (Fig. 3a). LV myocardial wall volume

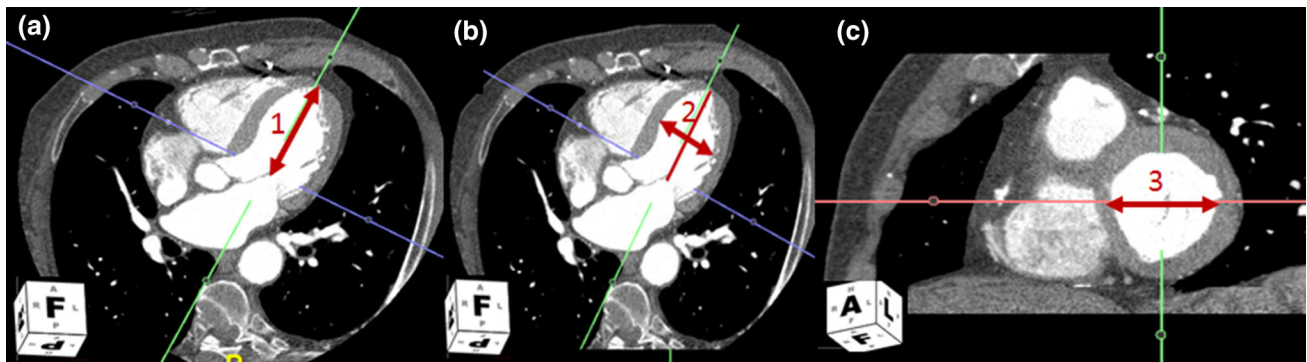


FIGURE 2. Cardiac 2D measures: (a) measure 1: LV long-axis length shown by the red arrow on the four-chamber view; the green line is aligned with the LV long-axis plane, (b) measure 2: LVEDD at 50% of LV long-axis length shown by the red arrow, (c) measure 3: LV short-axis length shown by the red arrow on the two-chamber view.

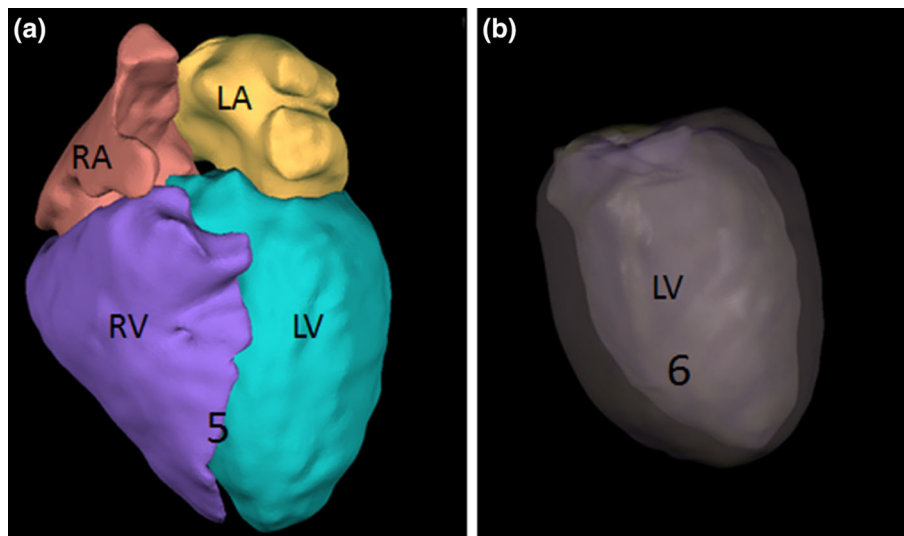


FIGURE 3. Cardiac 3D measures: (a) measure 5: Four chamber volumes: right atrium (RA), left atrium (LA), right ventricle (RV), and left ventricle (LV), (b) measure 6: LV myocardial wall volume.

was measured from a 3D model and normalized to the patient's BSA (Eq. 1; Fig. 3b).

Cardiothoracic Measures

The following cardiothoracic measures relating the location of the heart to other structures in the thoracic cavity were collected: (7) heart centroid to xipho-sternal junction distance, (8) closest path from the LV apex to intercostal space, (9) angle between the LV apex and intercostal space, (10) minimal distance between the sternum and heart, (11) angle between the mitral valve plane and LV long-axis, (12) angle between the LV long-axis and coronal plane (Figs. 4 and 5).

The heart centroid of all four chambers including the myocardium was calculated to measure the distance to the xipho-sternal junction (Fig. 4a). The resultant of two distance vectors from the LV apex to the nearest superior and inferior intercostal cartilage

defined the closest path from the LV apex to the intercostal space (Fig. 4b). The angle between this resultant vector and the anterior-posterior axis defined the angle between the LV apex and intercostal space (Fig. 4c).

The minimal distance between the sternum and heart was measured by placing a landmark on the xipho-sternal junction on the coronal view (Fig. 5a) and finding the closest path connecting the sternum to the myocardium on the sagittal view (Fig. 5b). The angle between the mitral valve plane and LV long-axis and the angle between the LV long-axis and coronal plane were measured on the four-chamber view (Fig. 5c).

Statistical Analysis

The mean, standard deviation, and range of the cardiothoracic measures were calculated, and student's *t*-tests were used to compare differences between sexes

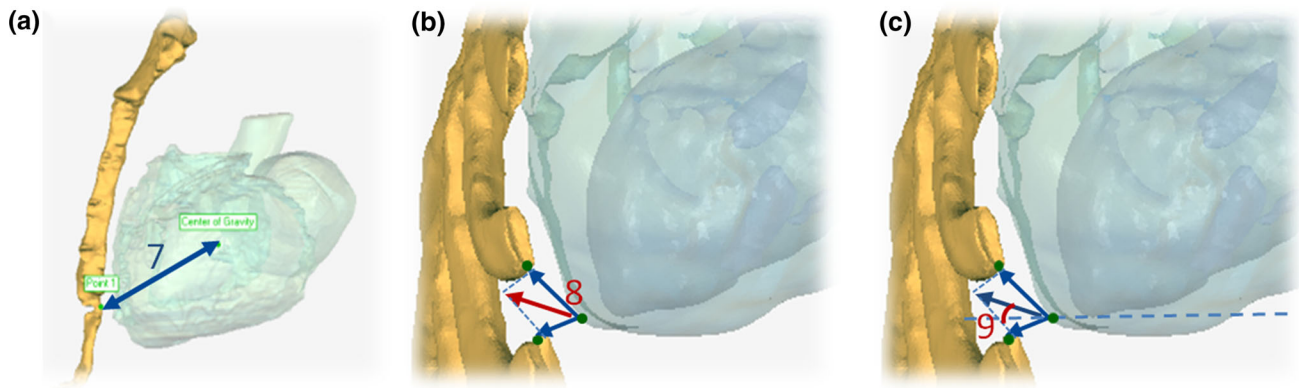


FIGURE 4. Cardiothoracic 3D measures: (a) measure 7: heart centroid to xipho-sternal junction distance, (b) measure 8: closest path from the LV apex to intercostal space, (c) measure 9: angle between the LV apex and intercostal space (angle between the anterior-posterior axis and the resultant vector from measure 8).

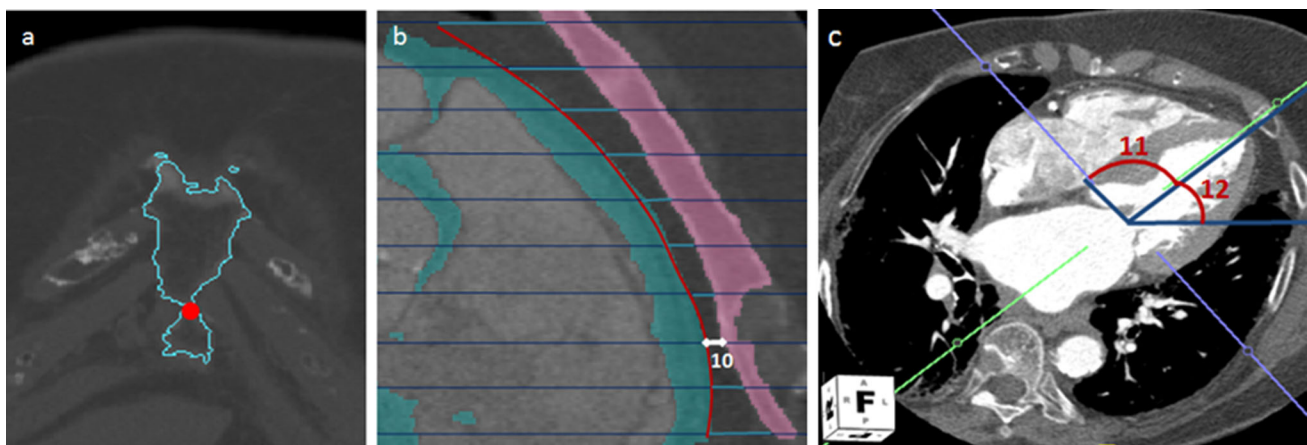


FIGURE 5. Cardiothoracic 2D measures: (a) xipho-sternal junction landmark on a coronal view, (b) measure 10: minimal distance between the sternum (pink) and heart (myocardium, cyan) shown by the white arrow on the sagittal view at the level of the xipho-sternal junction landmark; (c) measure 11: angle between the mitral valve plane and LV long-axis; measure 12: angle between the LV long-axis and coronal plane on the four-chamber view.

and between patients with reduced vs. preserved EF. Associations between each cardiothoracic measurement with another measurement, the patients' BSA, height, weight, and EF were examined using Pearson correlation coefficients. Using Bonferroni correction to adjust for multiple comparisons, an adjusted alpha level of 0.049 designated statistical significance in the t-tests and Pearson correlations. Statistical analysis was performed in JMP Pro 13 (*SAS Institute Inc., Cary, NC*).

RESULTS

Summary statistics for the 12 cardiothoracic measurements are provided in Table 2. Significant sex differences were observed in four cardiothoracic measures. LV long-axis length was significantly greater in males, and remained significant when normalized to

BSA ($p < 0.049$). LVEDD at 50% length of the long-axis was significantly greater in males, but was not significant when normalized to BSA. The minimal distance between the sternum and heart, and the angle between the LV long-axis and coronal plane, were also significantly greater in males.

EF was not significantly different between sexes, but four cardiothoracic measures differed between reduced vs. preserved EF patients. LV long-axis length and LVEDD were significantly greater in patients with reduced EF, and remained significant when normalized to BSA ($p < 0.049$). LV volume normalized to BSA was significantly greater in reduced EF patients. The angle between the mitral valve and LV long-axis was significantly greater in reduced EF patients, but did not remain significant when normalized to BSA.

Patients were categorized by the rib level of the intercostal space that generated the closest path to the LV apex (Fig. 6). The LV apex was nearest to the 5th

TABLE 2. Cardiothoracic measurements compared between males vs. females and reduced vs. preserved ejection fraction.

Measures	Mean ± SD	Min.	Max.	Female (n = 8)		Male (n = 12)		p-value	Preserved EF (n = 13)		Reduced EF (n = 7)		p-value
				Mean ± SD	Mean ± SD	Mean ± SD	Mean ± SD		Mean ± SD	Mean ± SD			
Cardiac measures													
1	Left ventricular long-axis length (mm)	77.4 ± 6.2	62.7	88.1	74.2 ± 5.0	79.5 ± 6.0	74.4 ± 4.1	0.028*	74.4 ± 4.1	82.8 ± 5.8	0.007*		
2	Left ventricular end-diastolic diameter at 50% of LV long-axis length (mm)	36.7 ± 8.2	24.8	50.0	31.2 ± 7.0	40.4 ± 8.0	33.6 ± 7.4	0.006*	33.6 ± 7.4	42.4 ± 6.4	0.015*		
3	Left ventricular short-axis length (mm)	45.6 ± 5.0	37.6	55.3	43.6 ± 2.3	46.9 ± 5.7	44.2 ± 4.6	0.103	44.2 ± 4.6	48.4 ± 5.0	0.121		
4	Left ventricular sphericity	1.7 ± 0.2	1.3	2.0	2.43 ± 0.37	2.0 ± 0.4	1.7 ± 0.16	0.880	1.7 ± 0.16	1.7 ± 0.23	0.641		
5	Left ventricular volume/body surface area (mL/m ²)	74.9 ± 34.8	46.1	175	68.4 ± 29	79.2 ± 38.0	57.8 ± 13.7	0.490	57.8 ± 13.7	106.8 ± 34.9	0.018*		
	Right ventricular volume/body surface area (mL/m ²)	71.6 ± 31.4	39.4	158	64.3 ± 33	57.6 ± 19.0	62.0 ± 16.1	0.790	62.0 ± 16.1	100.0 ± 40.3	0.153		
	Left atrial volume/body surface area (mL/m ²)	63.6 ± 10.1	45.8	81.2	67.4 ± 6.0	61.1 ± 12.0	61.75 ± 10.4	0.130	61.75 ± 10.4	67.3 ± 9.2	0.262		
	Right atrial volume/body surface area (mL/m ²)	60.3 ± 24.6	37.7	143	64.3 ± 33	57.6 ± 19	54.8 ± 10.6	0.610	54.8 ± 10.6	70.5 ± 38.8	0.333		
6	Left ventricular myocardial wall volume/body surface area (mL/m ²)	145.0 ± 31.2	103	230	153 ± 22	140 ± 36	139.8 ± 25.2	0.340	139.8 ± 25.2	154.7 ± 40.4	0.399		
Cardiothoracic measures													
7	Heart centroid to xipho-sternal junction distance (mm)	70.2 ± 11.9	51	92.5	69 ± 12	71 ± 12	71.8 ± 11.8	0.610	71.8 ± 11.8	67.3 ± 12.5	0.453		
8	Closest path from LV apex to intercostal space (mm)	37.4 ± 25.7	12.1	102	27.5 ± 10.8	44 ± 30.9	38.8 ± 28.0	0.615	38.8 ± 28.0	34.9 ± 22.8	0.745		
9	Angle between the LV apex and intercostal space (degree)	36.7 ± 25.1	1.6	82.7	42.5 ± 32.7	32.8 ± 19	37.7 ± 23.8	0.733	37.7 ± 23.8	34.8 ± 29.2	0.830		
10	Minimal distance between the sternum and heart (mm)	4.7 ± 3.0	1.4	12.3	3.41 ± 1.37	5.56 ± 3.56	4.8 ± 3.3	0.039*	4.8 ± 3.3	4.5 ± 2.8	0.815		
11	Angle between the mitral valve and LV long-axis (degree)	90.3 ± 6.5	78	102	89.8 ± 7.1	90.6 ± 6.3	87.7 ± 5.4	0.790	87.7 ± 5.4	95.0 ± 5.8	0.018*		
12	Angle between the LV long-axis and coronal plane (degree)	46.8 ± 9.5	28	66	40.1 ± 5.8	51.2 ± 5.5	48.2 ± 9.9	0.017*	48.2 ± 9.9	44.0 ± 8.9	0.349		

*Indicates significant difference between groups.

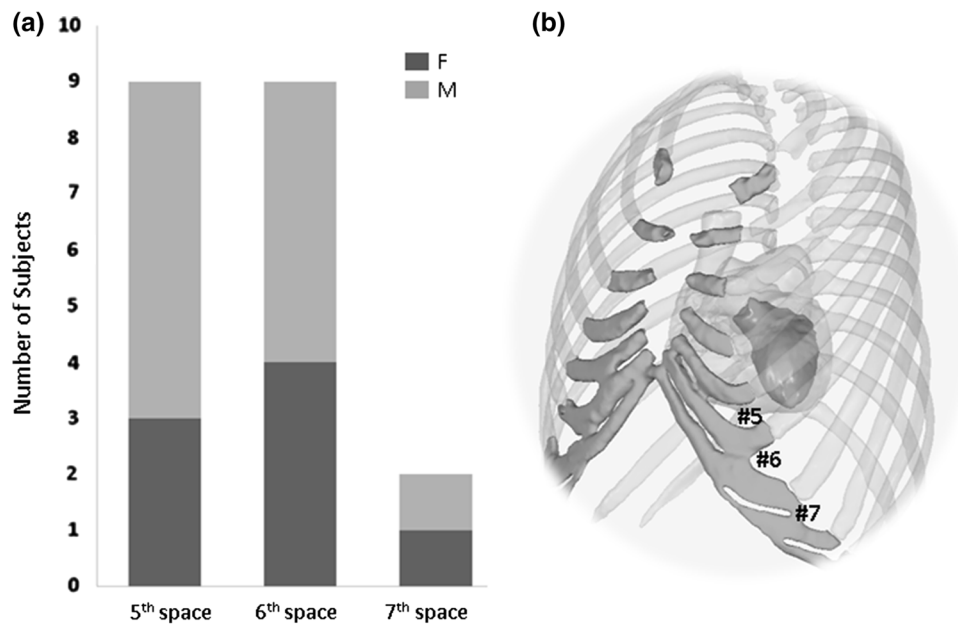


FIGURE 6. (a) Patients grouped by the closest path from the LV apex to the nearest intercostal space. (b) Intercostal space numbering in the 3D.

and 6th intercostal spaces in most of the patients, with approximately equal distribution between sexes.

EF was significantly correlated with LV long-axis length ($r = -0.52$; $p = 0.01$), LV volume/BSA ($r = -0.70$; $p < 0.01$), right ventricular volume/BSA ($r = -0.56$; $p = 0.04$), right atrial volume/BSA ($r = -0.62$; $p = 0.01$), and angle between the mitral valve and LV long-axis ($r = -0.52$; $p = 0.01$). LV short-axis length was significantly correlated with LVEDD ($r = 0.64$; $p < 0.01$), and LV volume/BSA ($r = 0.71$; $p < 0.01$). Minimal distance between the sternum and heart was correlated with BSA ($r = 0.46$, $p = 0.04$). LV volume/BSA was correlated with weight ($r = -0.53$, $p = 0.01$), BSA ($r = -0.48$, $p = 0.02$) and right ventricular volume/BSA ($r = 0.65$, $p = 0.02$). Left atrial volume/BSA was correlated with height ($r = -0.30$, $p = 0.03$). LV myocardial wall volume was correlated with weight ($r = -0.37$, $p = 0.01$), BSA ($r = -0.44$, $p = 0.01$) and LV volume/BSA ($r = 0.49$, $p < 0.01$). Angle between the LV apex and intercostal space was correlated with height ($r = -0.26$, $p = 0.04$). LVEDD was correlated with LV volume/BSA ($r = 0.56$, $p = 0.03$) and angle between the LV long-axis and coronal plane ($r = 0.39$, $p = 0.03$). LV sphericity was correlated with LV short axis length ($r = -0.73$, $p = 0.01$). BSA was correlated with weight ($r = 0.96$, $p < 0.01$) and height ($r = 0.62$, $p < 0.01$). All other correlations were not significant. Correlation coefficients and p -values from all correlation analyses are reported in supplementary material.

DISCUSSION

Cardiac Measures

In accordance with literature, LV long-axis length and LVEDD were significantly greater in males, while LV sphericity was not associated with sex.⁹ LV volume showed no correlation with sex in contrast to larger studies.⁹ Reduced EF patients had significantly greater LV long-axis length, LVEDD, and LV volume, even when normalized to body size. As all the reduced EF patients in this study were diagnosed with systolic dysfunction, the LV enlargement could be due to impaired emptying of the LV and reduced ability of the heart muscles to contract normally, producing an enlarged end-diastolic volume relative to stroke volume.¹⁴

Cardiothoracic Measures

The minimal distance between the sternum and heart averaged 4.7 ± 3.0 mm, and was 2.15 mm larger on average in males. Across the 20 patients, this distance ranged from 1.4 to 12.3 mm. Bypass grafts are recommended to be located > 10 mm from the sternum in patients for re-operative cardiothoracic surgeries.¹⁹ Our data provides an estimate of the gap between the heart and sternum for placing cardiovascular devices in this space which can prevent sternal adhesion and fatal arterial injuries²³ and bypass graft replacement.¹² The greater angle between the LV long-axis and coronal plane in males shows the heart is

more tilted anteriorly in the transverse plane in females.

The greater angle between the mitral valve and LV long-axis in reduced EF patients is possibly a result of a change in LV shape, which also increases the LV long-axis, LVEDD and LV volume.²¹ For these latter measures, reduced EF appears to affect LV morphology even when controlling for body size. The correlations of EF with LV long-axis length, LV volume, right ventricular volume, right atrial volume, and angle between the mitral valve and LV long-axis suggest an association with ventricular and atrial remodeling which are signs of HF progression.

Limitations

While the study provides exploratory data on the relationship between cardiothoracic morphology, sex, and ejection fraction in a cohort of HF patients, the small sample size limits generalizability of the results and may not capture the full range and variability of the HF patient population. Although likely underpowered, the study identified some significant differences in cardiothoracic morphology by sex and EF, and fills an important void in the literature by providing detailed cardiothoracic morphology data of prime relevance to cardiac device design. Although the non-gated chest CT scans had a lower resolution than the gated CT scans, co-registration compensated for lower resolution in the non-gated scans and a smaller field-of-view in the gated scans. The segmented models from chest scans were confirmed by two reviewers and the heart segmentations were reviewed by a medical imaging expert to reduce intra- and inter-observer variability.

Applications

Highly detailed anatomical models generated in this study can outperform 2D conventional cardiac measurements as structural complexities are captured in the 3D models. Although the patient sample is small due to the time-consuming image analysis that was performed, the morphological measures offer high resolution CT-derived data on HF patient variability which is of value to surgeons and device engineers. The pilot data reported in this study can be used to power studies in larger populations to validate results and inform clinical applications.

These cardiothoracic measurements and models could assist with surgical planning and the design of cardiac grafts, cardiac pacemakers, ventricular assist devices, and implantable defibrillators for HF management. To our knowledge, the cardiothoracic measures reported in this study have not been reported in any cardiac morphology study in this much detail. Appli-

cations of the study methodology could be used to develop real-time high resolution 3D models for surgical planning or patient-specific device development. The model development pipeline used in this study could be replicated by device design and surgical simulation engineers to optimize design specifications and improve surgical outcomes. For example, the closest path from the LV apex to intercostal space could help surgeons in point-of-entry identification during pre-surgical planning. This helps surgeons reduce time and improve efficiency in the operating room for complex surgeries. As another example, due to extreme variation in patient size in pediatric surgeries, the multi-modality image consolidation method could be used by surgical simulation engineers to provide morphological measures that help surgeons with anatomical demarcation and age-matched contour identification before surgery. In addition, in multi-stage surgeries for complex cases, the morphological data collected from the patient at each stage of the surgery can be consolidated into a single digital model to improve quality of patient and family education for better health outcomes.

Devices that are not patient-specific must be designed using inputs that characterize the range of anatomical conditions they must perform under in the population of their intended use. The morphological variability measures from this cohort can be used to test whether cardiac devices are appropriately sized and optimally engineered to be used in a broad array of HF patients. Quantitative evaluation of cardiothoracic morphology can inform design specifications for implants that must fit within a specific the cardiothoracic region. Ventricular assist devices are one example of a device with size requirements that can have a significant impact on the ease of implant and ultimate performance. Delivery tools used to access specific regions in and around the heart should have appropriate geometry and mechanical properties to ensure reliable performance across a wide range of anatomies. In addition, procedures used in conjunction with these delivery tools are crucial to patient outcomes. As procedures become less invasive, more detailed understanding of anatomical use conditions is required due to less flexibility in the approach.

Two applications commonly used during device development are computational modeling and bench testing. Information collected in this study informs both of these applications to ensure they are clinically relevant and provide useful feedback on device performance. If this information is not collected and used to inform these crucial tools, devices and associated implanted procedures run the risk of being designed in a way that does not meet the requirements of intended use. This results in poor patient outcomes and more cost to the health care system.

ELECTRONIC SUPPLEMENTARY MATERIAL

The online version of this article (<https://doi.org/10.1007/s13239-019-00436-z>) contains supplementary material, which is available to authorized users.

AUTHOR CONTRIBUTIONS

Study concept and design: Ryan Lahm, Ashley A. Weaver. Acquisition of data: Mona Saffarzadeh, James P. Gaewsky, Joshua Tan, Ashley A. Weaver. Analysis and interpretation: Mona Saffarzadeh, James P. Gaewsky, Bharathi Upadhy, Geoffrey T. Jao, Ryan Lahm, Ashley A. Weaver. Study supervision: Ryan Lahm, Ashley A. Weaver.

ACKNOWLEDGMENTS

The authors thank Caresse Hightower, Katelyn Greene, Elizabeth Lopez, Jennifer Dawkins, Casey Costa, and Xin Ye for their assistance with data collection. This work was supported by Medtronic [W-000617], and a National Science Foundation REU Site grant [Award No. 1559700].

ANIMAL STUDIES

No animal studies were carried out by the authors for this article.

CONFLICT OF INTEREST

Ashley A. Weaver report grants from Medtronic and the National Science Foundation during the conduct of the study. Ryan Lahm is an employee of Medtronic plc. Mona Saffarzadeh, James P. Gaewsky, Joshua Tan, Bharathi Upadhy, and Geoffrey T. Jao declare no conflict of interest.

HUMAN STUDIES/INFORMED CONSENT

All procedures followed were in accordance with the ethical standards of the responsible committee on human experimentation (institutional and national) and with the Helsinki Declaration of 1975, as revised in 2000 (5). The study complied with Institutional Review Board policies approved by Wake Forest University.

REFERENCES

- ¹Alberta, H. B., T. Takayama, T. C. Smits, B. B. Wendorff, R. P. Cambria, M. A. Farber, *et al.* Aortic arch morphology and aortic length in patients with dissection, traumatic, and aneurysmal disease. *Eur. J. Vasc. Endovasc. Surg.* 50(6):754–760, 2015. <https://doi.org/10.1016/j.ejvs.2015.08.005>.
- ²Asferg, C., L. Usinger, T. S. Kristensen, and J. Abdulla. Accuracy of multi-slice computed tomography for measurement of left ventricular ejection fraction compared with cardiac magnetic resonance imaging and two-dimensional transthoracic echocardiography: a systematic review and meta-analysis. *Eur. J. Radiol.* 81(5):e757–e762, 2012. <https://doi.org/10.1016/j.ejrad.2012.02.002>.
- ³Bak, S. H., S. M. Ko, H. J. Jeon, H. S. Yang, H. K. Hwang, and M. G. Song. Assessment of global left ventricular function with dual-source computed tomography in patients with valvular heart disease. *Acta Radiol.* 53(3):270–277, 2012. <https://doi.org/10.1258/ar.2011.1102.47>.
- ⁴Bennett, C. J., J. J. Maleszewski, and P. A. Araoz. CT and MR imaging of the aortic valve: radiologic-pathologic correlation. *Radiographics* 32(5):1399–1420, 2012. <https://doi.org/10.1148/rg.325115727>.
- ⁵Blair, J. E., M. Huffman, and S. J. Shah. Heart failure in North America. *Curr. Cardiol. Rev.* 9(2):128–146, 2013.
- ⁶Coats, A. J. The “muscle hypothesis” of chronic heart failure. *J. Mol. Cell Cardiol.* 28(11):2255–2262, 1996. <https://doi.org/10.1006/jmcc.1996.0218>.
- ⁷Geleijnse, M. L., P. M. Fioretti, and J. R. Roelandt. Methodology, feasibility, safety and diagnostic accuracy of dobutamine stress echocardiography. *J. Am. Coll. Cardiol.* 30(3):595–606, 1997.
- ⁸Gordon, E. P., I. Schnittger, P. J. Fitzgerald, P. Williams, and R. L. Popp. Reproducibility of left ventricular volumes by two-dimensional echocardiography. *J. Am. Coll. Cardiol.* 2(3):506–513, 1983.
- ⁹Gruner Svealv, B., G. Fritzson, and B. Andersson. Gender and age related differences in left ventricular function and geometry with focus on the long axis. *Eur. J. Echocardiogr.* 7(4):298–307, 2006. <https://doi.org/10.1016/j.euje.2005.06.008>.
- ¹⁰Halon, D. A., J. Ayman, R. Rubinshtein, B. Zafirir, M. Azencot, and B. S. Lewis. Cardiac computed tomography angiographic findings as predictors of late heart failure in an asymptomatic diabetic cohort: an 8-year prospective follow-up study. *Cardiology* 138(4):218–227, 2017. <https://doi.org/10.1159/000478995>.
- ¹¹Hayes, A. R., F. S. Gayzik, D. P. Moreno, R. S. Martin, and J. D. Stitzel. Abdominal organ location, morphology, and rib coverage for the 5(th), 50(th), and 95(th) percentile males and females in the supine and seated posture using multi-modality imaging. *Ann. Adv. Automot. Med.* 57:111–122, 2013.
- ¹²Heo, W., H. K. Min, D. K. Kang, H. J. Jun, Y. H. Hwang, and H. C. Lee. Three different situations and approaches in the management for anomalous origin of the right coronary artery from the left coronary sinus: case report. *J. Cardiothorac. Surg.* 9:21, 2014. <https://doi.org/10.1186/1749-8090-9-21>.

- ¹³Ho, S. Y., and P. Nihoyannopoulos. Anatomy, echocardiography, and normal right ventricular dimensions. *Heart* 92(Suppl 1):i2–i13, 2006.
- ¹⁴Iwano, H., and W. C. Little. Heart failure: what does ejection fraction have to do with it? *J. Cardiol.* 62(1):1–3, 2013. <https://doi.org/10.1016/j.jcc.2013.02.017>.
- ¹⁵Lam, C. S., P. Gona, M. G. Larson, J. Aragam, D. S. Lee, G. F. Mitchell, *et al.* Aortic root remodeling and risk of heart failure in the Framingham Heart study. *JACC Heart Fail.* 1(1):79–83, 2013. <https://doi.org/10.1016/j.jchf.2012.11.003>.
- ¹⁶Lu, M. T., H. Ersoy, A. G. Whitmore, M. J. Lipton, and F. J. Rybicki. Reformatted four-chamber and short-axis views of the heart using thin section (≤ 2 mm) MDCT images. *Acad. Radiol.* 14(9):1108–1112, 2007. <https://doi.org/10.1016/j.acra.2007.05.019>.
- ¹⁷Nishimura, R. A., C. M. Otto, R. O. Bonow, B. A. Carabello, J. P. Erwin, 3rd, R. A. Guyton, *et al.* 2014 AHA/ACC guideline for the management of patients with valvular heart disease: executive summary: a report of the American College of Cardiology/American Heart Association Task Force on Practice Guidelines. *Circulation* 129(23):2440–2492, 2014. <https://doi.org/10.1161/cir.000000000000029>.
- ¹⁸Owan, T. E., D. O. Hodge, R. M. Herges, S. J. Jacobsen, V. L. Roger, and M. M. Redfield. Trends in prevalence and outcome of heart failure with preserved ejection fraction. *N. Engl. J. Med.* 355(3):251–259, 2006. <https://doi.org/10.1056/NEJMoa052256>.
- ¹⁹Rajiah, P., and P. Schoenhagen. The role of computed tomography in pre-procedural planning of cardiovascular surgery and intervention. *Insights Imaging.* 4(5):671–689, 2013. <https://doi.org/10.1007/s13244-013-0270-8>.
- ²⁰Raman, S. V., M. Shah, B. McCarthy, A. Garcia, and A. K. Ferketich. Multi-detector row cardiac computed tomography accurately quantifies right and left ventricular size and function compared with cardiac magnetic resonance. *Am. Heart J.* 151(3):736–744, 2006. <https://doi.org/10.1016/j.ahj.2005.04.029>.
- ²¹Rizvi, A., R. C. Deaño, D. P. Bachman, G. Xiong, J. K. Min, and Q. A. Truong. Analysis of ventricular function by CT. *J. Cardiovasc Comput. Tomogr.* 9(1):1–12, 2015. <https://doi.org/10.1016/j.jcct.2014.11.007>.
- ²²Shuman, W. P., K. R. Branch, J. M. May, L. M. Mitsumori, D. W. Lockhart, T. J. Dubinsky, *et al.* Prospective versus retrospective ECG gating for 64-detector CT of the coronary arteries: comparison of image quality and patient radiation dose. *Radiology* 248(2):431–437, 2008. <https://doi.org/10.1148/radiol.2482072192>.
- ²³Stark, J. The use of valved conduits in pediatric cardiac surgery. *Pediatric Cardiol.* 19(4):282–288, 1998. <https://doi.org/10.1007/s002469900311>.
- ²⁴The Criteria Committee of the New York Heart Association. Nomenclature and criteria for diagnosis of diseases of the heart and great vessels. 9th ed. Boston: Little, Brown, 1994.
- ²⁵Zile, M. R., J. S. Gottdiener, S. J. Hetzel, J. J. McMurray, M. Komajda, R. McKelvie, *et al.* Prevalence and significance of alterations in cardiac structure and function in patients with heart failure and a preserved ejection fraction. *Circulation* 124(23):2491–2501, 2011. <https://doi.org/10.1161/CIRCULATIONAHA.110.011031>.

Publisher's Note Springer Nature remains neutral with regard to jurisdictional claims in published maps and institutional affiliations.